
MTTB: End-to-End Framework for Oxide TFT Channel Guidelines Beyond-IGZO

Anonymous Author(s)

Affiliation

Address

email

Abstract

As AMOLED displays move toward higher resolution and lower power operation, next-generation oxide semiconductors are needed to achieve high-performance, reliable backplane TFTs. However, existing ML-based screening has two limitations. It can distort design decisions by collapsing conflicts among multiple material descriptors into a single objective function. It also lacks an interpretable link between material-level predictions and device-level performance. To address these issues, we propose a four-stage hybrid framework, *MTTB* (Materials-to-TFT Bridge). (1) **AI-based property prediction**: rapidly infers material descriptors (band gap G_x , inverse spatial wavefunction overlaps $ISWO_C$ and $ISWO_V$, and formation energy E_f) from composition vectors. (2) **Pareto-based multi-objective composition search**: compresses promising candidates while preserving trade-offs among material descriptors. (3) **Candidate selection strategy**: selects final candidate compositions based on performance–stability trade-offs and target priorities. (4) **Physics-Inference Module (PIM)**: maps predicted properties to device-physics variables to efficiently infer TCAD-equivalent device metrics. Experimentally, global Pareto-knee candidates converge to Al–Mg-centered compositions under high-bandgap conditions. Composition-sensitivity analysis and PIM-based device simulations confirm the potential for balanced performance improvements over IGZO. Finally, we propose Al–Mg-based (beyond-IGZO) oxide archetypes and composition candidates that can replace IGZO.

21

1 Introduction

22 AMOLED (Active-Matrix Organic Light-Emitting Diode) displays offer high contrast and fast
23 response. They are widely used as a core display technology in electronic devices, including
24 smartphones (1). As demand increases for higher resolution and lower-power operation, requirements
25 for the electrical performance and stability of AMOLED driving devices continue to intensify (2).
26 Meeting these requirements requires thin-film transistors (TFTs) in the AMOLED backplane to
27 provide both sufficient current-driving capability and long-term reliability (3).

28 Oxide TFTs exhibit higher carrier mobility and lower leakage current than amorphous silicon (a-Si)
29 TFTs. Among them, indium–gallium–zinc oxide (IGZO) has been successfully commercialized and
30 is now the most widely used representative material (4; 5). However, continued improvements in
31 display performance require exploring multicomponent oxide materials beyond IGZO (5). The key
32 challenge is the exponential growth of the design space as elemental combinations diversify. Con-
33 ventional experiment-driven approaches alone are insufficient for identifying optimal compositions
34 (6). Accordingly, high-speed screening frameworks that combine material-descriptor calculations
35 (bandgap, $ISWO$, E_f) with machine learning (ML), such as the work of Kim *et al.* (2022) (14), have
36 emerged as a key methodology for accelerating next-generation materials discovery.

37 However, while these approaches help reduce the composition space, they have two fundamental
38 limitations when linking predicted material properties to TFT device performance.

39 First, many ML-based screening methods integrate multiple material descriptors into a single objective
40 function. This can fail to capture intrinsic physical trade-offs among bandgap, formation energy, and
41 electronic localization (e.g., ISWO). For example, low formation energy suggests thermodynamic
42 stability. However, if it accompanies excessive oxygen vacancies, it can reduce the bandgap and
43 destabilize the threshold voltage (9). Collapsing multivariate trade-offs into a single scalar objective
44 can prematurely exclude physically plausible compositions or yield unrealistic optima. Practical
45 composition exploration therefore requires a multi-objective optimization framework that preserves
46 balance among multiple material descriptors while refining the design space (10).

47 Second, many ML frameworks stop at composition or property prediction. Even when they predict
48 device performance, they often rely on black-box models that do not explicitly reveal the underlying
49 physical mechanisms (7). Commercial TCAD simulations can mitigate this issue, but their high
50 computational cost limits repeated evaluation of large candidate sets (8). Some studies directly learn
51 correlations between composition and device performance, but they do not sufficiently provide an
52 interpretable link describing how changes in electronic structure map to device-physics variables
53 (device parameters), such as carrier concentration or trap density (8).

54 The main contributions of this paper are summarized as follows.

- 55 • **MTTB framework:** We propose a four-stage hybrid framework, *MTTB* (Materials-to-TFT
56 Bridge). It consists of (i) **AI-based material prediction**, (ii) Pareto-based multi-objective
57 composition search, (iii) Candidate selection strategy, and (iv) a Physics-inference module.
- 58 • **Addressing two fundamental limitations of prior ML-based approaches:** We address two
59 limitations of prior ML-based screening studies. First, collapsing conflicting relationships
60 among multiple material descriptors into a single objective can distort design decisions. We
61 mitigate this using Pareto-based multi-objective optimization and decision rules. Second,
62 many studies do not provide an explicit link between material-level predictions and device-
63 level performance. We address this via the PIM.
- 64 • **Actionable beyond-IGZO candidates:** We apply MTTB to an Al–Mg-centered multi-
65 component oxide composition space. We derive IGZO-replacement compositions that
66 globally balance trade-offs among bandgap, mobility, and stability. We also provide specific
67 next-generation (beyond-IGZO) compositions for follow-up experimental validation.

68 2 Related work

69 **ML-based discovery of amorphous oxide materials** van Setten *et al.* (14) proposed a framework
70 that combines HT-DFT with support vector regression (SVR) models. It efficiently screens the
71 composition space of amorphous multicomponent oxides. They learned composition–property
72 relationships from computed data for primary and binary oxides. They then generalized the models
73 to multicomponent (multinary) systems. This enabled prediction of key metrics such as bandgap
74 and formation energy. They also prioritized promising composition regions to reduce search cost.
75 They further demonstrated that the framework can propose new candidates. As an IGZO replacement
76 candidate, they suggested Zn–Mg–Al–O (ZMAO). However, the approach has limitations. It is not
77 an end-to-end workflow from material-property prediction to device-performance validation. It does
78 not explicitly capture trade-offs among material descriptors because it relies on single-objective
79 optimization. It also remains limited in scalability for large-batch parallel processing over large
80 composition spaces.

81 3 Preliminary

82 3.1 Material Descriptors

83 To link atomic-scale electronic structure to device performance, we define four material descriptors,
84 $\mathbf{x} = [G_x, ISWO_C, ISWO_V, E_f]$. The bandgap G_x is defined as $G_x = E_{CBM} - E_{VBM}$ and
85 is closely related to leakage current and charge-injection barriers; a larger G_x is favorable for
86 suppressing off-state leakage and improving visible-light transmittance.

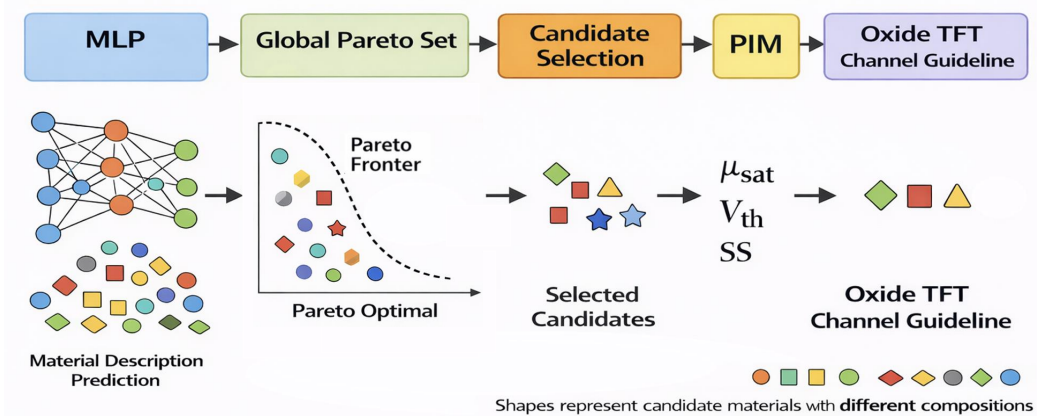


Figure 1: Overview of the MTTB framework.

- 87 Inverse Spatial Wavefunction Overlap (ISWO) is defined as the inverse of the orbital overlap integral
 88 S ($ISWO \propto S^{-1}$). A smaller $ISWO_C$ indicates greater delocalization of conduction-band electron
 89 wavefunctions and thus higher electron mobility, whereas a larger $ISWO_V$ suppresses hole transport
 90 in the valence band and is favorable for n-type behavior.
 91 The formation energy E_f is defined as the total energy difference normalized by the number of oxygen
 92 atoms, $E_f = \Delta E_{tot}/N_O$, and reflects thermodynamic stability. Values lower than or comparable to
 93 IGZO indicate suppressed phase separation and reduced defect formation during processing.
 94 To assess the de-mixing tendency of mixed amorphous oxides, we adopt the formation-energy-based
 95 stability metric E_{hull} proposed by van Setten *et al.* (14). Here, $E_{\text{hull}} < 0$ indicates that the mixed
 96 state is thermodynamically more stable than separation into constituent single oxides. In this study,
 97 E_{hull} is used only as a post hoc stability filter for Pareto-selected candidates.

98 3.2 TFT Performance Metrics

99 We summarize TFT electrical behavior using three metrics: mobility (μ_{sat}), threshold voltage (V_{th}),
 100 and subthreshold swing (SS). μ_{sat} is the effective mobility extracted from the current characteristics
 101 in the saturation regime. It directly affects switching speed and on-current. V_{th} is the gate voltage at
 102 which the channel forms and the drain current begins to increase substantially. It is a key parameter
 103 for low-power operation. SS is the gate-voltage change required for the drain current to increase by
 104 one decade in the subthreshold regime. It is calculated as $SS = \partial V_{GS}/\partial(\log I_{DS})$.

105 4 Method

106 In this section, we present the MTTB framework, which integrates AI-based material property
 107 prediction, Pareto-based multi-objective screening, and physics-informed device-level inference. An
 108 overview of the framework is shown in Fig. 1.

109 4.1 AI-based Material Property Prediction

110 4.1.1 Dataset Description

111 We used the amorphous oxide dataset reported in prior work (14), which comprises amorphous
 112 oxide properties computed using high-precision DFT. Amorphous structures were generated from
 113 local bonding motifs derived from unary ($X-O$) and binary ($X-Y-O$) crystalline structures in
 114 the Materials Project, with strictly stoichiometric compositions to exclude extrinsic n-type doping.
 115 Each unit cell contained approximately 200 atoms, and DFT calculations were performed on 10
 116 independent amorphous configurations per composition to ensure statistical robustness. The dataset
 117 covers amorphous oxides composed of 12 metal elements (Ag, Al, Cd, Ga, In, Mg, Sb, Si, Sn, Ti, Zn,
 118 and Zr).

119 **4.1.2 MLP-based predictor**

120 To address the limited expressiveness of the SVR model used in prior work, we adopt a two-layer
121 multi-layer perceptron (MLP) to capture nonlinear relationships in high-dimensional composition
122 space. The input is a normalized metal composition vector, and the model is designed for rapid
123 inference without requiring explicit atomic-structure information.

124 Given the heterogeneous distributions and learning difficulties of different target properties, we
125 trained independent MLPs for each property. The models predict four descriptors: bandgap (E_g),
126 formation energy (E_f), $ISWO_C$, and $ISWO_V$. This design enables fast batch inference over large
127 composition sets, significantly improving the efficiency of subsequent multi-objective screening.

128 **4.2 Pareto-based Multi-objective Composition Optimization**

129 **4.2.1 Rationale for Pareto Optimization in Materials Design**

130 A weight-based single-objective function that compresses multiple properties into a single scalar
131 can simplify the search. However, such an approach inherently fails to preserve explicit trade-offs
132 between objectives (14). To address this, we treat each property as an independent objective and
133 adopt a multi-objective optimization strategy to derive the Pareto-optimal set.

134 A Pareto-optimal set consists of solutions for which no objective can be improved without degrading
135 at least one other. The resulting Pareto front delineates the boundary of potentially optimal candidate
136 compositions while preserving the intrinsic trade-off structure among properties. This approach is
137 particularly effective for materials design problems that must simultaneously consider competing
138 requirements, such as electronic performance and stability (10; 23; 24).

139 **4.2.2 Search Space Definition and Composition Sampling**

140 We defined the composition search space by generating all binary ($X-Y-O$) and ternary ($X-Y-Z-$
141 O) oxide combinations that can be formed by selecting two or three elements from the 12-element
142 set. Within each system, candidate compositions were generated via Dirichlet-distribution-based
143 sampling. We used 30 compositions per ternary system and 15 compositions per binary system. To
144 reflect practical controllability in deposition processes, we excluded trace components with an atomic
145 fraction below 0.01% during sampling.

146 **4.2.3 Objective Function Formulation**

147 All objectives were formulated as minimization problems. For each candidate composition, we defined
148 four objectives:

$$f_1 = (E_{gap} - (E_{gap,IGZO} + \Delta E_{target}))^2, \quad f_2 = ISWO_C, \quad f_3 = -ISWO_V, \quad f_4 = E_f.$$

149 We set $\Delta E_{target} \in \{0.0, 0.25, 0.50, 0.75, 1.00\}$. We considered $\Delta E_{target} \in$
150 $\{0.0, 0.25, 0.50, 0.75, 1.00\}$. These objectives jointly capture electronic properties, carrier
151 transport, and thermodynamic stability. The Pareto front of non-dominated solutions was then
152 computed, enabling systematic selection of candidates that balance performance and stability beyond
153 single-property criteria.

154 **4.2.4 Hierarchical Pareto Screening and Global Front Construction**

155 We first computed local Pareto fronts independently for each binary and ternary composition system.
156 System-level Pareto candidates were then aggregated across all binary systems and across all ternary
157 systems to construct order-wise global Pareto fronts.

158 Next, a formation-energy-based de-mixing stability metric (E_{hull}) was applied to the binary and
159 ternary Pareto candidate sets. Only compositions with no tendency toward phase separation in the
160 mixed state ($Stability < 0$) were retained. Composition ratios were rounded to two decimal places
161 to remove duplicates, and for identical chemical formulas, the candidate with the lowest de-mixing
162 energy was kept. Finally, the filtered binary and ternary candidates were merged into a single set, and
163 Pareto optimization was performed once more to obtain the final global Pareto set spanning the full
164 composition space. From the global Pareto set (822 compositions), we formed candidate sets under
165 three distinct criteria.

166 **4.3 Candidate Selection Strategy from the Global Pareto Set**

167 **Property-prioritized Candidate Buckets** Because industrial requirements do not reduce to a
168 single property, we partitioned the merged global Pareto set into three candidate buckets reflecting
169 different property priorities. The high-mobility bucket selects the top five compositions with the
170 smallest $ISWO_C$ under target bandgap and stability constraints, whereas the high-stability bucket
171 selects the top five compositions with the lowest formation energy E_f while maintaining charge-
172 transport properties. The balanced bucket applies a multi-criteria ranking that sequentially considers
173 bandgap proximity, formation energy, and $ISWO_C$. This analysis serves as a supplementary tool for
174 comparing candidate distributions under different property-driven design scenarios.

175 **Bandgap-conditioned Knee Point Selection** Next, for each target bandgap, we identified curvature-
176 based knee points on the corresponding Pareto front to extract compromise candidates. Four objective
177 functions—bandgap proximity, mobility, reliability, and formation energy—were normalized to the
178 $[0, 1]$ range, and the sacrifice rate between adjacent candidates was computed. The knee point was
179 defined as the candidate with the maximum sacrifice rate, characterizing locally optimal solutions for
180 each bandgap condition.

181 **Global Knee-based Final Selection** Finally, in the normalized four-dimensional objective space
182 that integrates all bandgap targets, we computed the Euclidean distance to the utopia point $(0, 0, 0, 0)$.
183 We define the 20 compositions with the smallest global distances as the global-knee set. These
184 candidates are considered to provide the most effective global compromise among bandgap, mobility,
185 and stability. In this study, we propose the global-knee set as the primary target for subsequent
186 device-physics simulations and experimental validation.

187 **4.4 Physics-Inference Module (PIM)**

188 We propose a Physics-Inference Module (PIM) that estimates device-level TCAD inputs and TFT
189 electrical metrics from AI-predicted DFT material descriptors. Key features of the PIM include:

- 190 • **Relative anchor:** IGZO DFT predictions are used as a reference, and the target composition
191 is interpreted through relative deviations, constraining inferred parameters to physically
192 plausible ranges.
- 193 • **Physics-grounded linkage:** DFT descriptors are mapped to device parameters and subse-
194 quently to $I-V_g$ characteristics to extract μ_{sat} , V_{th} , and SS .
- 195 • **Computational efficiency:** The physics-based mapping bypasses iterative TCAD simula-
196 tions, enabling rapid evaluation of large candidate sets.

197 Specifically, based on semiconductor physics, the bandgap G_x is mapped to a variable related to the
198 intrinsic carrier concentration (16). The relative change in $ISWO_C$ is used as a proxy for changes
199 in electron transport and mobility. Deviations in $ISWO_V$ and E_f are converted into parameters
200 that reflect changes in the distribution of defect/trap states. These parameters are reflected in the
201 trap density and threshold-voltage variation. The estimated physical variables are then fed into an
202 exponential model in the subthreshold regime and a gradual-channel-approximation model in strong
203 inversion. This generates TFT transfer characteristics ($I-V_g$) (16; 17). Finally, we apply a parameter-
204 extraction algorithm to the generated $I-V_g$ to extract μ_{sat} , V_{th} , and SS (22). Implementation details
205 are provided in our released code.

206 **Scope and limitations of the PIM.** The PIM serves as a physics-informed surrogate for device-level
207 evaluation, rather than a replacement for full TCAD simulations. Its mappings are based on simplified,
208 relative, and IGZO-anchored relationships, and therefore do not capture detailed electrostatics, spatial
209 defect distributions, or process-dependent variations. Accordingly, the PIM is intended for efficient
210 comparative screening and trend analysis, while final quantitative validation requires rigorous TCAD
211 or experimental verification.

212 **5 Experiment**

213 In this section, we evaluate the proposed framework by addressing the following research questions:
214 **RQ1.** Does the model accurately generalize across diverse oxide compositions?

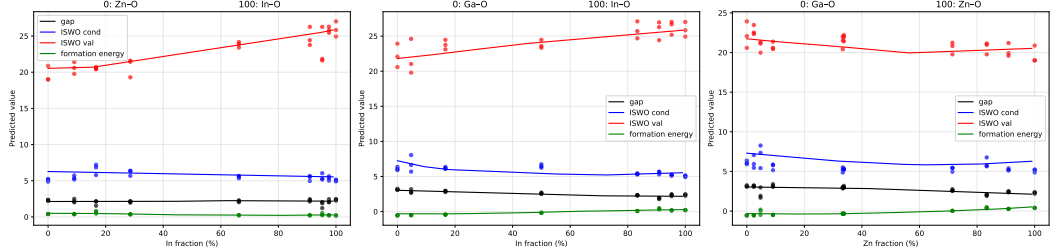


Figure 2: Validation of physical trends. Solid lines and scatter points denote MLP predictions and DFT calculations, respectively, for the In-Ga-Zn-O system.

Table 1: Comparison of property prediction performance across models.

Target (y)	Gaussian			van Setten <i>et al.</i> (14)			Ours		
	MAE	Corr	R^2	MAE	Corr	R^2	MAE	Corr	R^2
G_x	0.216	0.962	-0.214	0.256	0.369	-0.594	0.186	0.379	-0.037
E_f	0.944	0.351	-16.326	0.019	0.995	0.986	0.026	0.994	0.976
$ISWO_V$	2.599	-0.143	-14.712	1.160	-0.134	-2.295	1.132	0.462	0.183
$ISWO_C$	1.130	0.455	0.201	1.184	0.457	0.056	0.966	0.137	-0.969
Avg.	1.222	0.406	-7.763	0.654	0.422	-0.461	0.577	0.493	0.038

- 215 **RQ2.** How do optimal oxide systems shift across varying bandgap requirements?
 216 **RQ3.** How can Pareto-optimal candidates be categorized for device requirements?
 217 **RQ4.** What is the ultimate material archetype for high-performance oxide semiconductors?
 218 **RQ5.** How robust is the Al–Mg archetype against composition variations?
 219 **RQ6.** Do AI-designed oxide TFT channels deliver gains under TCAD validation?

220 5.1 Experimental Settings

221 The framework was implemented in Python 3.12 (18) using PyTorch 2.9 (19) and executed on Google
 222 Colab (20) with an NVIDIA T4 GPU (21). PIM-based TCAD-equivalent analyses (Section 4.4) were
 223 performed under the following device and operating conditions. All evaluations were conducted at
 224 room temperature ($T \approx 300$ K), consistent with standard oxide TFT characterization protocols (4; 5;
 225 3). The channel geometry was set to $W = 50\text{ }\mu\text{m}$ and $L = 10\text{ }\mu\text{m}$, with a gate insulator thickness
 226 of $t_{ox} = 20$ nm. The relative permittivity of the gate insulator was fixed at $\epsilon_{r,ox} = 10$, and the
 227 oxide capacitance was calculated using the standard MOS expression, $C_{ox} = \epsilon_{r,ox}\epsilon_0/t_{ox}$ (16; 17).
 228 The implementation of the proposed MTTB framework is available at <https://anonymous.4open.science/r/MTTB-228F/>.
 229

230 5.2 Generalization Performance of the Prediction Model

231 We evaluated the model’s generalization performance using quantitative metrics (Table 1) and physical
 232 consistency. On the unseen Mg–Zn–Al oxide dataset, the proposed model achieved the lowest error
 233 among the compared methods (mean MAE = 0.577) and attained positive values for $ISWO_V$ and
 234 the overall mean R^2 , where prior models failed. This demonstrates reliable prediction performance
 235 for complex multicomponent systems. In a composition sweep of the In–Ga–Zn (IGZO) system
 236 (Fig. 2), the model accurately reproduced key physical trends: $ISWO_C$ improved with increasing
 237 In content, while the bandgap (E_g) widened with increasing Ga content. Smooth interpolation in
 238 data-sparse regions indicates that the model stably captures the underlying physical landscape shaped
 239 by inter-element correlations, supporting its qualitative reliability for multicomponent composition
 240 exploration.

Table 2: Summary of dominant systems and predicted property ranges by target ΔE_g .

Target ΔE_g (eV)	Representative Element	E_g (eV)	$ISWO_C$	Stability
0.00	Ag, Zr, Ti	0.14–0.56	16.5–18.4	≈ -3.0
0.25	Mg, Ti, Al	2.75–2.81	29.8–31.2	≈ -2.8
0.50	Zr, Cd, In, Sn	2.96–3.03	21.1–24.5	≈ -3.4
0.75	Al, Ga, Zn, Zr	3.26–3.30	17.1–21.3	-1.8–2.8
1.00	Al, Mg, Sb	3.43–3.68	8.0–9.3	≈ -2.1

Table 3: Statistical summary of material properties by performance bucket.

Bucket	ΔE_g (eV)		$ISWO_C$		E_f		Stability	
	Mean	Std	Mean	Std	Mean	Std	Mean	Std
balanced	3.02	0.36	18.80	8.67	-2.41	1.09	-0.39	0.23
high_mobility	2.90	0.44	6.17	0.73	-0.77	0.51	-0.34	0.24
high_stability	3.03	0.28	27.88	1.81	-3.99	0.19	-0.24	0.10

241 5.3 System Transitions Across Bandgap Regimes

242 We identify distinct system transitions in which dominant elemental combinations shift abruptly at
243 specific thresholds (Table 2).

244 **Low-bandgap regime ($\Delta E_g \approx 0.0$ eV).** Ag–Zr-based systems dominate, maintaining high conductivity while leveraging Zr to ensure minimal amorphous-structure stability.

245 **Intermediate transition regime ($\Delta E_g = 0.25$ – 0.75 eV).** Ag-based systems vanish near $\Delta E_g \approx$
246 0.25 eV, and the optimum shifts to Mg–Ti systems, reflecting a trade-off in which mobility ($ISWO_C$)
247 is partially sacrificed to secure a wider bandgap via lightweight-metal-based stabilization. At higher
248 targets, a Zr-based backbone re-emerges, combined with elements such as In, Sn, and Ga to restore
249 the mobility–stability balance and maximize design flexibility.

250 **High-bandgap regime ($\Delta E_g \approx 1.0$ eV).** The strategy converges to an Al–Mg backbone, with strong
251 gap openers such as Sb, signaling entry into a property regime suitable for dielectric or barrier layers
252 beyond semiconductor channels.

254 5.4 Device-requirement-driven Candidate Categorization

255 To recommend optimal compositions aligned with user design objectives within the Pareto solution
256 set, we analyzed candidates in three performance-oriented buckets (Table 3).

257 **High Mobility:** Dominated by the In–Ga–Zn family, this bucket maximizes *s*-orbital overlap and
258 achieves the lowest $ISWO_C$ (≈ 6.17), at the cost of reduced bandgap and higher formation energy.

259 **High Stability:** Strong bonding driven primarily by Zr (63%) and Ti (23%) yields the lowest
260 formation energy (≈ -3.99 eV). However, the increased ionicity limits conduction-band overlap,
261 resulting in suppressed mobility.

262 **Balanced:** All property metrics converge to intermediate values. This regime reflects a cooperative
263 design strategy, with Zr contributing stability, In/Ga/Zn enhancing transport, and Al/Mg enabling
264 bandgap tuning.

265 5.5 Emergence of an Al–Mg Archetype in Global Pareto Optima

266 We analyzed the 20 global optima (Global Knee) obtained by integrating all bandgap targets. As
267 shown in Fig. 4a, unlike bucket-based candidates biased toward either mobility or stability, the Global
268 Knee candidates cluster at the optimal compromise between these properties, occupying a region
269 with markedly lower formation energy and superior $ISWO_C$ relative to the IGZO baseline.

270 Notably, all 20 global optima emerge at the maximum bandgap requirement, $\Delta E_g = 1.0$ eV (i.e.,
271 $E_g \approx$ IGZO + 1.0 eV; Fig. 3), indicating that high-bandgap conditions impose strong physical
272 constraints to maintain charge transport and structural stability. These extreme constraints act as a
273 physical filter that drives the Pareto knee to converge to a specific composition region.

Table 4: Statistical summary of Global Knee candidates ($n = 20$).

(a) System distribution and property ranges.				(b) Elemental composition statistics.			
System	Count	ΔE_{gap}	$ISWO_C$	Stability	Element	Mean	Std
(Al, Mg)	5	3.80–4.27	9.01–10.19	–2.64––2.25	Al	0.5285	0.1254
(Al, In, Mg)	4	3.59–4.03	8.47–9.57	–2.52––2.24	Mg	0.4420	0.1204
(Al, Ga, Mg)	3	3.83–4.10	9.10–9.76	–2.53––2.28	In	0.0080	0.0217
(Al, Mg, Si)	3	3.82–4.04	9.03–9.45	–2.39––2.26	Zr	0.0075	0.0217
(Al, Mg, Zr)	2	3.79–3.83	9.50–12.86	–2.69––2.29	Si	0.0075	0.0185

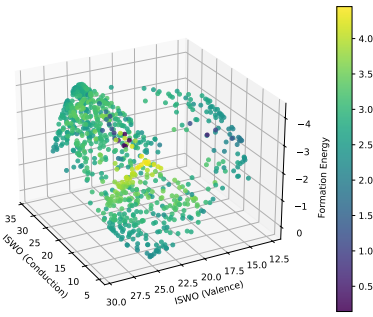


Figure 3: 3D global Pareto sets across all bandgap targets.

274 Consistently, the Global Knee systems share a common Al–Mg backbone (Table 4a), with Al and Mg
 275 accounting for approximately 97% of the total composition (Table 4b), suggesting convergence to a
 276 near-binary Al–Mg oxide archetype under the most stringent property requirements.

277 5.6 Composition Robustness of the Al–Mg Oxide Archetype

278 From the composition distributions of the global-knee optimal systems, we observe a flat region when
 279 the Al fraction exceeds 0.55, where material properties remain nearly invariant despite changes in the
 280 Mg:X ratio (Fig. 5). This indicates that the third element functions as a dopant, fine-tuning target
 281 properties without perturbing the underlying backbone.

282 As a result, the global optimum converges to a variable dopant configuration on a robust Al–Mg
 283 backbone. Higher Al content further suppresses sensitivity to composition variations, providing a
 284 practical materials design guideline for achieving high yield in large-area AMOLED manufacturing.

285 5.7 Device-level Validation of AI-designed Oxide TFT Channels

286 We performed PIM-based TCAD simulations to evaluate the practical utility of the AI-proposed
 287 compositions (Fig. 4b).

288 **IGZO baseline validation:** For commercial IGZO ($In_{50}Ga_{50}Zn_{50}$), we obtained $V_{th} = 0.95$ V and
 289 $\mu = 15.0 \text{ cm}^2/\text{V} \cdot \text{s}$. These values are consistent with typical experimental reports, supporting the
 290 reliability of the simulation setup.

291 **Device performance of Global Knee candidates:** The 20 global-optimal candidates showed strong
 292 statistical advantages over IGZO across all metrics. We obtained approximately 76% higher mobility
 293 ($\mu_{avg} \approx 26.4$) and excellent switching behavior ($SS_{avg} \approx 128.6 \text{ mV/dec}$).

294 **Process reproducibility:** The threshold voltage is densely distributed within the operating window
 295 ($V_{th} = 2.26 \pm 0.23$ V), indicating high uniformity for large-area processing.

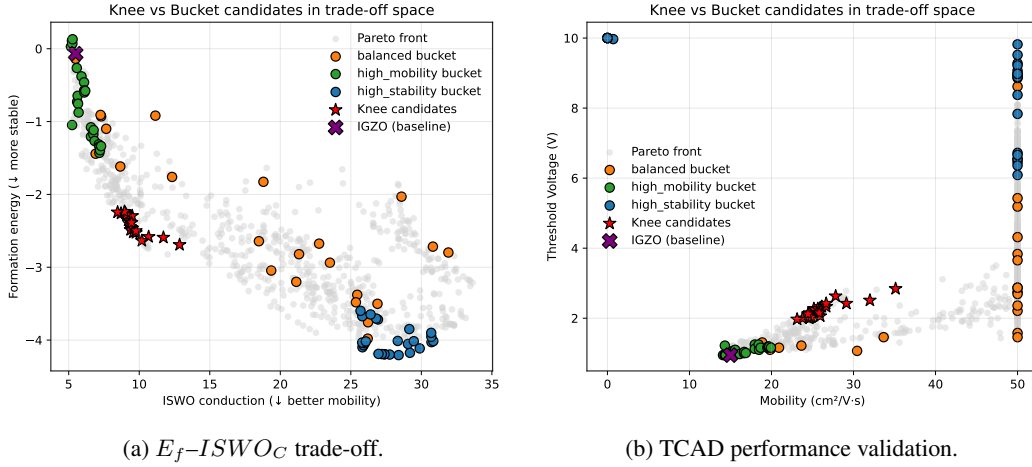


Figure 4: Global distribution and performance of Pareto results.

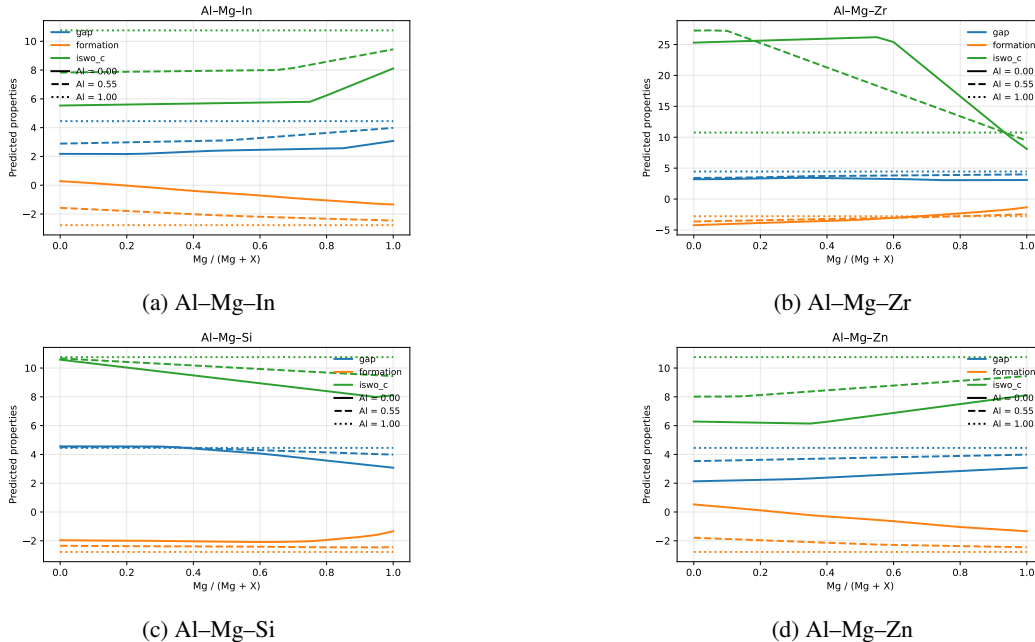


Figure 5: Fine-tuning effects of ternary elements (In, Zr, Si, Zn).

296 6 Conclusion

297 This study addresses the challenge of identifying oxide TFT channel materials that can replace IGZO
 298 to meet the high-performance and high-reliability demands of next-generation AMOLED backplanes.
 299 We propose the *MTTB* framework, which integrates composition-based property prediction, Pareto-
 300 based multi-objective screening, and TCAD-level device-performance inference via the Physics-
 301 Inference Module (PIM). Under stringent requirements such as a high bandgap, the design space is
 302 shown to converge to an Al–Mg binary archetype. We further demonstrate that Al–Mg–X systems
 303 exhibit low sensitivity to composition variations while enabling dopant-based fine-tuning, providing
 304 robust oxide TFT channel design guidelines for large-area AMOLED manufacturing. These systems
 305 also indicate improved device-performance potential compared with conventional IGZO.

306 The proposed framework supports physically consistent decision-making from material candidate
 307 discovery to device-performance validation and can be extended to incorporate process variables and
 308 device-stack-level co-design.

309 **References**

- 310 [1] J.-H. Lee *et al.*, “Recent progress in organic light-emitting diodes for display applications,”
311 *Advanced Materials*, vol. 32, no. 34, 2002840, 2020.
- 312 [2] S. Reineke, “Complementary LED technologies,” *Nature Materials*, vol. 12, pp. 474–475, 2013.
- 313 [3] E. Fortunato, P. Barquinha, and R. Martins, “Oxide semiconductor thin-film transistors: a review
314 of recent advances,” *Advanced Materials*, vol. 24, no. 22, pp. 2945–2986, 2012.
- 315 [4] K. Nomura *et al.*, “Room-temperature fabrication of transparent flexible thin-film transistors
316 using amorphous oxide semiconductors,” *Nature*, vol. 432, no. 7016, pp. 488–492, 2004.
- 317 [5] T. Kamiya, K. Nomura, and H. Hosono, “Present status of amorphous In–Ga–Zn–O thin-film
318 transistors,” *Science and Technology of Advanced Materials*, vol. 11, no. 4, 044305, 2010.
- 319 [6] P. Raccuglia *et al.*, “Machine-learning-assisted materials discovery using failed experiments,”
320 *Nature*, vol. 533, no. 7601, pp. 73–76, 2016.
- 321 [7] K. T. Butler *et al.*, “Machine learning for molecular and materials science,” *Nature*, vol. 559,
322 no. 7715, pp. 547–555, 2018.
- 323 [8] Q. Ding, A. V. Kuhlmann, A. Fuhrer, and A. Schenk, “A Generalizable TCAD Framework for
324 Silicon FinFET Spin Qubit Devices with Electrical Control,” arXiv:2306.03213, 2023.
- 325 [9] D.-G. Kim *et al.*, “Negative threshold voltage shift in an a-IGZO thin film transistor under X-ray
326 irradiation,” *RSC Advances*, vol. 9, pp. 20865–20870, 2019.
- 327 [10] K. Deb, A. Pratap, S. Agarwal, and T. Meyarivan, “A fast and elitist multiobjective genetic
328 algorithm: NSGA-II,” *IEEE Transactions on Evolutionary Computation*, vol. 6, no. 2, pp. 182–
329 197, 2002.
- 330 [11] A. Jain *et al.*, “Commentary: The Materials Project: A materials genome approach to accelerat-
331 ing materials innovation,” *APL Materials*, vol. 1, no. 1, 011002, 2013.
- 332 [12] L. Ward *et al.*, “Matminer: An open source toolkit for materials data mining,” *Computational
333 Materials Science*, vol. 152, pp. 60–69, 2018.
- 334 [13] S. Curtarolo *et al.*, “The high-throughput highway to computational materials design,” *Nature
335 Materials*, vol. 12, pp. 191–201, 2013.
- 336 [14] M. J. van Setten *et al.*, “Complex amorphous oxides: property prediction from high throughput
337 DFT and AI for new material search,” *Materials Advances*, vol. 3, pp. 8413–8427, 2022.
- 338 [15] T. D. K"uhne *et al.*, “CP2K: An electronic structure and molecular dynamics software package –
339 Quickstep: Efficient and accurate electronic structure calculations,” *The Journal of Chemical
340 Physics*, vol. 152, 194103, 2020.
- 341 [16] S. M. Sze and K. K. Ng, *Physics of Semiconductor Devices*, 3rd ed. Wiley, 2006.
- 342 [17] Y. Tsividis and C. McAndrew, *Operation and Modeling of the MOS Transistor*, 3rd ed. Oxford
343 University Press, 2011.
- 344 [18] Python Software Foundation, *Python Language Reference*, version 3.12, 2023.
- 345 [19] A. Paszke *et al.*, “PyTorch: An Imperative Style, High-Performance Deep Learning Library,” in
346 *Advances in Neural Information Processing Systems (NeurIPS)*, 2019.
- 347 [20] Google Research, *Google Colaboratory*, online platform documentation, accessed 2026.
- 348 [21] NVIDIA Corporation, *NVIDIA T4 Tensor Core GPU*, product brief/datasheet, 2018.
- 349 [22] A. Biswas and P. Schalberger, “PyTFT: Automated extraction of TFT parameters for simulation,”
350 software repository, University of Stuttgart, 2023.

351 [23] A. M. Gopakumar, P. V. Balachandran, D. Xue, J. E. Gubernatis, and T. Lookman, “Multi-
352 objective Optimization for Materials Discovery via Adaptive Design,” *Scientific Reports*, vol. 8,
353 3738, 2018.

354 [24] K. M. Jablonka, G. M. Jothiappan, S. Wang, B. Smit, and B. Yoo, “Bias free multiobjective
355 active learning for materials design and discovery,” *Nature Communications*, vol. 12, 2312,
356 2021.

357 **A Appendix / supplemental material**

358 Optionally include supplemental material (complete proofs, additional experiments and plots) in
359 appendix. All such materials **SHOULD be included in the main submission.**

360 **AI Co-Scientist Challenge Korea Paper Checklist**

361 **1. Claims**

362 Question: Do the main claims made in the abstract and introduction accurately reflect the
363 paper's contributions and scope?

364 Answer: [Yes]

365 Justification: The abstract and introduction clearly state the four-stage MTTB framework,
366 the motivation (limitations of single-objective ML screening), and the scope (beyond-IGZO
367 oxide TFT channels), all of which are consistently supported by the proposed methods and
368 experimental results.

369 Guidelines:

- 370 • The answer NA means that the abstract and introduction do not include the claims
371 made in the paper.
- 372 • The abstract and/or introduction should clearly state the claims made, including the
373 contributions made in the paper and important assumptions and limitations. A No or
374 NA answer to this question will not be perceived well by the reviewers.
- 375 • The claims made should match theoretical and experimental results, and reflect how
376 much the results can be expected to generalize to other settings.
- 377 • It is fine to include aspirational goals as motivation as long as it is clear that these goals
378 are not attained by the paper.

379 **2. Limitations**

380 Question: Does the paper discuss the limitations of the work performed by the authors?

381 Answer: [Yes]

382 Justification: The paper explicitly clarifies the scope and limitations of the Physics-Inference
383 Module (PIM), stating that it is a physics-informed surrogate rather than a full TCAD
384 replacement, and that it relies on simplified, IGZO-anchored mappings which do not capture
385 detailed electrostatics or process-dependent effects.

386 Guidelines:

- 387 • The answer NA means that the paper has no limitation while the answer No means that
388 the paper has limitations, but those are not discussed in the paper.
- 389 • The authors are encouraged to create a separate "Limitations" section in their paper.
- 390 • The paper should point out any strong assumptions and how robust the results are to
391 violations of these assumptions (e.g., independence assumptions, noiseless settings,
392 model well-specification, asymptotic approximations only holding locally). The authors
393 should reflect on how these assumptions might be violated in practice and what the
394 implications would be.
- 395 • The authors should reflect on the scope of the claims made, e.g., if the approach was
396 only tested on a few datasets or with a few runs. In general, empirical results often
397 depend on implicit assumptions, which should be articulated.
- 398 • The authors should reflect on the factors that influence the performance of the approach.
399 For example, a facial recognition algorithm may perform poorly when image resolution
400 is low or images are taken in low lighting. Or a speech-to-text system might not be
401 used reliably to provide closed captions for online lectures because it fails to handle
402 technical jargon.
- 403 • The authors should discuss the computational efficiency of the proposed algorithms
404 and how they scale with dataset size.
- 405 • If applicable, the authors should discuss possible limitations of their approach to
406 address problems of privacy and fairness.
- 407 • While the authors might fear that complete honesty about limitations might be used by
408 reviewers as grounds for rejection, a worse outcome might be that reviewers discover
409 limitations that aren't acknowledged in the paper. The authors should use their best
410 judgment and recognize that individual actions in favor of transparency play an impor-
411 tant role in developing norms that preserve the integrity of the community. Reviewers
412 will be specifically instructed to not penalize honesty concerning limitations.

413 **3. Theory Assumptions and Proofs**

414 Question: For each theoretical result, does the paper provide the full set of assumptions and
415 a complete (and correct) proof?

416 Answer: [N/A]

417 Justification: The paper does not present formal theorems or mathematical proofs; it is
418 primarily a framework and methodology paper combining ML, multi-objective optimization,
419 and physics-informed modeling.

420 Guidelines:

- 421 • The answer NA means that the paper does not include theoretical results.
- 422 • All the theorems, formulas, and proofs in the paper should be numbered and cross-
423 referenced.
- 424 • All assumptions should be clearly stated or referenced in the statement of any theorems.
- 425 • The proofs can either appear in the main paper or the supplemental material, but if
426 they appear in the supplemental material, the authors are encouraged to provide a short
427 proof sketch to provide intuition.
- 428 • Inversely, any informal proof provided in the core of the paper should be complemented
429 by formal proofs provided in appendix or supplemental material.
- 430 • Theorems and Lemmas that the proof relies upon should be properly referenced.

431 **4. Experimental Result Reproducibility**

432 Question: Does the paper fully disclose all the information needed to reproduce the main ex-
433 perimental results of the paper to the extent that it affects the main claims and/or conclusions
434 of the paper (regardless of whether the code and data are provided or not)?

435 Answer: [Yes]

436 Justification: The paper specifies datasets, model architecture (MLP), objective formulations,
437 Pareto procedures, PIM mappings, and experimental settings, and additionally provides an
438 anonymized code repository to support reproducibility.

439 Guidelines:

- 440 • The answer NA means that the paper does not include experiments.
- 441 • If the paper includes experiments, a No answer to this question will not be perceived
442 well by the reviewers: Making the paper reproducible is important, regardless of
443 whether the code and data are provided or not.
- 444 • If the contribution is a dataset and/or model, the authors should describe the steps taken
445 to make their results reproducible or verifiable.
- 446 • Depending on the contribution, reproducibility can be accomplished in various ways.
447 For example, if the contribution is a novel architecture, describing the architecture fully
448 might suffice, or if the contribution is a specific model and empirical evaluation, it may
449 be necessary to either make it possible for others to replicate the model with the same
450 dataset, or provide access to the model. In general, releasing code and data is often
451 one good way to accomplish this, but reproducibility can also be provided via detailed
452 instructions for how to replicate the results, access to a hosted model (e.g., in the case
453 of a large language model), releasing of a model checkpoint, or other means that are
454 appropriate to the research performed.
- 455 • While AI Co-Scientist Challenge Korea does not require releasing code, the conference
456 does require all submissions to provide some reasonable avenue for reproducibility,
457 which may depend on the nature of the contribution. For example
 - 458 (a) If the contribution is primarily a new algorithm, the paper should make it clear how
459 to reproduce that algorithm.
 - 460 (b) If the contribution is primarily a new model architecture, the paper should describe
461 the architecture clearly and fully.
 - 462 (c) If the contribution is a new model (e.g., a large language model), then there should
463 either be a way to access this model for reproducing the results or a way to reproduce
464 the model (e.g., with an open-source dataset or instructions for how to construct
465 the dataset).

466 (d) We recognize that reproducibility may be tricky in some cases, in which case
467 authors are welcome to describe the particular way they provide for reproducibility.
468 In the case of closed-source models, it may be that access to the model is limited in
469 some way (e.g., to registered users), but it should be possible for other researchers
470 to have some path to reproducing or verifying the results.

471 **5. Open access to data and code**

472 Question: Does the paper provide open access to the data and code, with sufficient instruc-
473 tions to faithfully reproduce the main experimental results, as described in supplemental
474 material?

475 Answer: [Yes]

476 Justification: The paper provides a public, anonymized repository link containing the
477 implementation and instructions, satisfying open-access and anonymity requirements at
478 submission time.

479 Guidelines:

- 480 • The answer NA means that paper does not include experiments requiring code.
- 481 • Please see the NeurIPS code and data submission guidelines (<https://nips.cc/public/guides/CodeSubmissionPolicy>) for more details.
- 482 • While we encourage the release of code and data, we understand that this might not be
483 possible, so “No” is an acceptable answer. Papers cannot be rejected simply for not
484 including code, unless this is central to the contribution (e.g., for a new open-source
485 benchmark).
- 486 • The instructions should contain the exact command and environment needed to run to
487 reproduce the results. See the NeurIPS code and data submission guidelines (<https://nips.cc/public/guides/CodeSubmissionPolicy>) for more details.
- 488 • The authors should provide instructions on data access and preparation, including how
489 to access the raw data, preprocessed data, intermediate data, and generated data, etc.
- 490 • The authors should provide scripts to reproduce all experimental results for the new
491 proposed method and baselines. If only a subset of experiments are reproducible, they
492 should state which ones are omitted from the script and why.
- 493 • At submission time, to preserve anonymity, the authors should release anonymized
494 versions (if applicable).
- 495 • Providing as much information as possible in supplemental material (appended to the
496 paper) is recommended, but including URLs to data and code is permitted.

497 **6. Experimental Setting/Details**

500 Question: Does the paper specify all the training and test details (e.g., data splits, hyper-
501 parameters, how they were chosen, type of optimizer, etc.) necessary to understand the
502 results?

503 Answer: [Yes]

504 Justification: The paper details the dataset composition, prediction targets, evaluation
505 metrics, device geometry, operating conditions, and computational environment, enabling
506 clear interpretation of the results.

507 Guidelines:

- 508 • The answer NA means that the paper does not include experiments.
- 509 • The experimental setting should be presented in the core of the paper to a level of detail
510 that is necessary to appreciate the results and make sense of them.
- 511 • The full details can be provided either with the code, in appendix, or as supplemental
512 material.

513 **7. Experiment Statistical Significance**

514 Question: Does the paper report error bars suitably and correctly defined or other appropriate
515 information about the statistical significance of the experiments?

516 Answer: [No]

517 Justification: Although averages and distributions are reported, the paper does not systematically provide confidence intervals, error bars, or formal statistical significance tests for the experimental comparisons.
518
519

520 Guidelines:

- 521 • The answer NA means that the paper does not include experiments.
- 522 • The authors should answer "Yes" if the results are accompanied by error bars, confi-
523 dence intervals, or statistical significance tests, at least for the experiments that support
524 the main claims of the paper.
- 525 • The factors of variability that the error bars are capturing should be clearly stated (for
526 example, train/test split, initialization, random drawing of some parameter, or overall
527 run with given experimental conditions).
- 528 • The method for calculating the error bars should be explained (closed form formula,
529 call to a library function, bootstrap, etc.)
- 530 • The assumptions made should be given (e.g., Normally distributed errors).
- 531 • It should be clear whether the error bar is the standard deviation or the standard error
532 of the mean.
- 533 • It is OK to report 1-sigma error bars, but one should state it. The authors should
534 preferably report a 2-sigma error bar than state that they have a 96% CI, if the hypothesis
535 of Normality of errors is not verified.
- 536 • For asymmetric distributions, the authors should be careful not to show in tables or
537 figures symmetric error bars that would yield results that are out of range (e.g. negative
538 error rates).
- 539 • If error bars are reported in tables or plots, The authors should explain in the text how
540 they were calculated and reference the corresponding figures or tables in the text.

541 8. Experiments Compute Resources

542 Question: For each experiment, does the paper provide sufficient information on the com-
543 puter resources (type of compute workers, memory, time of execution) needed to reproduce
544 the experiments?

545 Answer: [Yes]

546 Justification: The paper specifies the software stack, execution environment (Google Colab),
547 GPU type (NVIDIA T4), and general computational setup for the experiments.

548 Guidelines:

- 549 • The answer NA means that the paper does not include experiments.
- 550 • The paper should indicate the type of compute workers CPU or GPU, internal cluster,
551 or cloud provider, including relevant memory and storage.
- 552 • The paper should provide the amount of compute required for each of the individual
553 experimental runs as well as estimate the total compute.
- 554 • The paper should disclose whether the full research project required more compute
555 than the experiments reported in the paper (e.g., preliminary or failed experiments that
556 didn't make it into the paper).

557 9. Code Of Ethics

558 Question: Does the research conducted in the paper conform, in every respect, with the
559 NeurIPS Code of Ethics <https://nips.cc/public/EthicsGuidelines>?

560 Answer: [Yes]

561 Justification: The work involves materials modeling and simulation without human subjects,
562 personal data, or ethically sensitive applications, and preserves anonymity as required.

563 Guidelines:

- 564 • The answer NA means that the authors have not reviewed the NeurIPS Code of Ethics.
- 565 • If the authors answer No, they should explain the special circumstances that require a
566 deviation from the Code of Ethics.
- 567 • The authors should make sure to preserve anonymity (e.g., if there is a special consid-
568 eration due to laws or regulations in their jurisdiction).

569 **10. Broader Impacts**

570 Question: Does the paper discuss both potential positive societal impacts and negative
571 societal impacts of the work performed?

572 Answer: [Yes]

573 Justification: Although the paper does not include a standalone “Broader Impacts” section, it
574 explicitly clarifies that the PIM is a physics-informed surrogate intended only for comparative
575 screening, not for final decision-making. This implicitly addresses responsible use by
576 preventing overinterpretation or misuse of surrogate predictions, while the overall framework
577 supports positive industrial impact through more efficient and resource-aware materials
578 exploration.

579 Guidelines:

- 580 • The answer NA means that there is no societal impact of the work performed.
- 581 • If the authors answer NA or No, they should explain why their work has no societal
582 impact or why the paper does not address societal impact.
- 583 • Examples of negative societal impacts include potential malicious or unintended uses
584 (e.g., disinformation, generating fake profiles, surveillance), fairness considerations
585 (e.g., deployment of technologies that could make decisions that unfairly impact specific
586 groups), privacy considerations, and security considerations.
- 587 • The conference expects that many papers will be foundational research and not tied
588 to particular applications, let alone deployments. However, if there is a direct path to
589 any negative applications, the authors should point it out. For example, it is legitimate
590 to point out that an improvement in the quality of generative models could be used to
591 generate deepfakes for disinformation. On the other hand, it is not needed to point out
592 that a generic algorithm for optimizing neural networks could enable people to train
593 models that generate Deepfakes faster.
- 594 • The authors should consider possible harms that could arise when the technology is
595 being used as intended and functioning correctly, harms that could arise when the
596 technology is being used as intended but gives incorrect results, and harms following
597 from (intentional or unintentional) misuse of the technology.
- 598 • If there are negative societal impacts, the authors could also discuss possible mitigation
599 strategies (e.g., gated release of models, providing defenses in addition to attacks,
600 mechanisms for monitoring misuse, mechanisms to monitor how a system learns from
601 feedback over time, improving the efficiency and accessibility of ML).

602 **11. Safeguards**

603 Question: Does the paper describe safeguards that have been put in place for responsible
604 release of data or models that have a high risk for misuse (e.g., pretrained language models,
605 image generators, or scraped datasets)?

606 Answer: [N/A]

607 Justification: The released assets are materials design models and simulations with no clear
608 dual-use or misuse risk.

609 Guidelines:

- 610 • The answer NA means that the paper poses no such risks.
- 611 • Released models that have a high risk for misuse or dual-use should be released with
612 necessary safeguards to allow for controlled use of the model, for example by requiring
613 that users adhere to usage guidelines or restrictions to access the model or implementing
614 safety filters.
- 615 • Datasets that have been scraped from the Internet could pose safety risks. The authors
616 should describe how they avoided releasing unsafe images.
- 617 • We recognize that providing effective safeguards is challenging, and many papers do
618 not require this, but we encourage authors to take this into account and make a best
619 faith effort.

620 **12. Licenses for existing assets**

621 Question: Are the creators or original owners of assets (e.g., code, data, models), used in
622 the paper, properly credited and are the license and terms of use explicitly mentioned and
623 properly respected?

624 Answer: [Yes]

625 Justification: The paper properly cites prior datasets, software tools, and libraries, and
626 references their original publications.

627 Guidelines:

- 628 • The answer NA means that the paper does not use existing assets.
- 629 • The authors should cite the original paper that produced the code package or dataset.
- 630 • The authors should state which version of the asset is used and, if possible, include a
631 URL.
- 632 • The name of the license (e.g., CC-BY 4.0) should be included for each asset.
- 633 • For scraped data from a particular source (e.g., website), the copyright and terms of
634 service of that source should be provided.
- 635 • If assets are released, the license, copyright information, and terms of use in the
636 package should be provided. For popular datasets, paperswithcode.com/datasets
637 has curated licenses for some datasets. Their licensing guide can help determine the
638 license of a dataset.
- 639 • For existing datasets that are re-packaged, both the original license and the license of
640 the derived asset (if it has changed) should be provided.
- 641 • If this information is not available online, the authors are encouraged to reach out to
642 the asset's creators.

643 13. New Assets

644 Question: Are new assets introduced in the paper well documented and is the documentation
645 provided alongside the assets?

646 Answer: [Yes]

647 Justification: The MTTB framework and PIM are clearly described, and accompanying code
648 and documentation are provided in the repository.

649 Guidelines:

- 650 • The answer NA means that the paper does not release new assets.
- 651 • Researchers should communicate the details of the dataset/code/model as part of their
652 submissions via structured templates. This includes details about training, license,
653 limitations, etc.
- 654 • The paper should discuss whether and how consent was obtained from people whose
655 asset is used.
- 656 • At submission time, remember to anonymize your assets (if applicable). You can either
657 create an anonymized URL or include an anonymized zip file.

658 14. Crowdsourcing and Research with Human Subjects

659 Question: For crowdsourcing experiments and research with human subjects, does the paper
660 include the full text of instructions given to participants and screenshots, if applicable, as
661 well as details about compensation (if any)?

662 Answer: [N/A]

663 Justification: The study does not involve human participants or crowdsourced data.

664 Guidelines:

- 665 • The answer NA means that the paper does not involve crowdsourcing nor research with
666 human subjects.
- 667 • Including this information in the supplemental material is fine, but if the main contribu-
668 tion of the paper involves human subjects, then as much detail as possible should be
669 included in the main paper.
- 670 • According to the NeurIPS Code of Ethics, workers involved in data collection, curation,
671 or other labor should be paid at least the minimum wage in the country of the data
672 collector.

673 **15. Institutional Review Board (IRB) Approvals or Equivalent for Research with Human
674 Subjects**

675 Question: Does the paper describe potential risks incurred by study participants, whether
676 such risks were disclosed to the subjects, and whether Institutional Review Board (IRB)
677 approvals (or an equivalent approval/review based on the requirements of your country or
678 institution) were obtained?

679 Answer: [N/A]

680 Justification: No human-subject research is conducted, so IRB approval is not applicable.

681 Guidelines:

- 682 • The answer NA means that the paper does not involve crowdsourcing nor research with
683 human subjects.
- 684 • Depending on the country in which research is conducted, IRB approval (or equivalent)
685 may be required for any human subjects research. If you obtained IRB approval, you
686 should clearly state this in the paper.
- 687 • We recognize that the procedures for this may vary significantly between institutions
688 and locations, and we expect authors to adhere to the NeurIPS Code of Ethics and the
689 guidelines for their institution.
- 690 • For initial submissions, do not include any information that would break anonymity (if
691 applicable), such as the institution conducting the review.